HHS Public Access

Author manuscript

Brain Inj. Author manuscript; available in PMC 2015 May 21.

Published in final edited form as:

Brain Inj. 2015 ; 29(4): 438–445. doi:10.3109/02699052.2014.989907.

Longitudinal quantification and visualization of intracerebral hemorrhage using multimodal magnetic resonance and diffusion tensor imaging

S.Y. Matthew Goh[1], **Andrei Irimia**[1], **Carinna M. Torgerson**[1], **Meral A. Tubi**[2], **Courtney R. Real**[2], **Daniel F. Hanley**[3], **Neil A. Martin**[2], **Paul M. Vespa**[2], and **John D. Van Horn**[1,*]

[1]Institute for Neuroimaging and Informatics, Department of Neurology, Keck School of Medicine, University of Southern California

[2]Brain Injury Research Center, Department of Neurosurgery, David Geffen School of Medicine, University of California, Los Angeles

[3]Department of Neurology, John Hopkins University

Abstract

Objective—To demonstrate a set of approaches using diffusion tensor imaging (DTI) tractography whereby pathology-affected white matter (WM) fibers in patients with intracerebral hemorrhage (ICH) can be selectively visualized.

Methods—Using structural neuroimaging and DTI volumes acquired longitudinally from three representative ICH patients, the spatial configuration of ICH-related trauma is delineated and the WM fiber bundles intersecting each ICH lesion are identified and visualized. Both the extent of ICH lesions as well as the proportion of WM fibers intersecting the ICH pathology are quantified and compared across subjects.

Results—Our method successfully demonstrates longitudinal volumetric differences in ICH lesion load and differences across time in percentage of fibers which intersect the primary injury.

Conclusions—Because neurological conditions such as intracerebral hemorrhage (ICH) frequently exhibit pathology-related effects which lead to the exertion of mechanical pressure upon surrounding tissues, and thereby to the deformation and/or displacement of WM fibers, DTI fiber tractography is highly suitable for assessing longitudinal changes in WM fiber integrity and mechanical displacement.

Keywords

intracerebral hemorrhage; magnetic resonance imaging; diffusion tensor imaging; longitudinal study

[*]corresponding author: John D. Van Horn, Ph.D., The Institute for Neuroimaging and Informatics, Keck School of Medicine, University of Southern California, 2001 North Soto Street, Room 102, MC 9232, Los Angeles CA 90089-9235, USA, Phone: (01) 323-442-7246, Fax: (01) 323-442-7247, jvanhorn@usc.edu.

Declarations of interest: The authors declare no actual or potential competing conflicts of interest.

Introduction

Intracerebral hemorrhage (ICH) is a neurological condition whose occurrence can have profound implications for patient health and recovery. Spontaneous ICH is typically caused by hypertension, which can produce micro-aneurysms at the bifurcation of arterioles [1]. In clinical settings, ICH is frequently associated with poor patient outcome, with over 70% of patients experiencing residual motor deficits [2,3]. Approximately one third of ICH patients who receive a computed tomography (CT) scan within 3 hours of injury onset exhibit hematoma expansion on follow-up CT scans [4], suggesting that neuroimaging is critical to the assessment of injury progression and to the determination of treatment steps necessary for optimal recovery. While some studies based on CT neuroimaging have demonstrated the predictive correlation between hemorrhage volume and patient mortality [5], morbidity in the context of motor outcome is not consistently reflected by CT measurements due to the fact that many neural fibers involved in motor control are confined within relatively small areas and are thus susceptible to mechanical pressure [2]. In fact, it has been shown that pressure applied to white matter (WM) may cause fiber deformations and lead to significant loss of neuronal transmission, to demyelination, and to axonal shearing [6]. In the representative case of the corticospinal tract (CST), even a small volumetric extent of ICH may have severe debilitating effects [2]. Based on this knowledge, methodologies which can reveal the integrity of peri-lesional WM tracts can be beneficial in establishing a more comprehensive view of injury dynamics.

Whereas conventional structural magnetic resonance imaging (MRI) sequences such as fluid attenuated inversion recovery (FLAIR) and gradient recalled echo (GRE) imaging can reveal important structural information including the presence of edema and hemorrhage, the integrity of WM tracts is often better observed using diffusion tensor imaging (DTI) [7-13]. Many investigators have utilized DTI to extract quantitative metrics of ICH which are predictively correlated with motor outcome [2,14,15]. In addition, DTI tractography allows for the three-dimensional reconstruction of WM tracts, which greatly enhances the visual and quantitative exploration of fiber integrity. In the case of the CST, Jung and Jang [14] have investigated the relationships between the location and severity of injury along this tract, on the one hand, and motor outcome, on the other hand. The combination of tractography and 3D anatomical models derived from structural imaging volumes can be used to assess longitudinal changes in WM tracts, particularly from the standpoint of how affected fibers are displaced and may subsequently recover over time. By means of freely-available neuroimage analysis software packages such as 3D Slicer (slicer.org), TrackVis (trackvis.org) and the LONI Pipeline (pipeline.loni.usc.edu), this case study evaluation demonstrates the versatility of 3D ICH modeling and DTI fiber tractography in the context of longitudinal visualization and quantification of ICH. The usefulness of the paradigm and its applicability to the clinical assessment of this condition are illustrated in three representative clinical cases of ICH.

Methods

Patients and image acquisition

Multimodal neuroimaging volumes were acquired from three patients with spontaneous ICH at the Ronald Reagan Medical Center of the University of California, Los Angeles (UCLA). Informed written consent was provided either by the subjects themselves or by their authorized legal representatives, and neuroimage volume acquisition was conducted with the approval of the Institutional Review Board of the School of Medicine at UCLA. Patients 1, 2 and 3 (ages: 63, 56 and 44, respectively) were admitted to the neurointensive care unit (NICU) with Glasgow Coma Scores (GCS) of 14, 6 and 7, respectively, and discharged with GCS scores of 11, 7 and 6, respectively. All three patients received an initial MRI scan within twelve hours of admission. Patient 1 underwent thrombolytic therapy and received a follow up scan 15 days after the injury date. Patient 2 underwent endoscopic evacuation of the hemorrhage and received a follow up scan three days after the injury. Patient 3 underwent endoscopic evacuation and received three additional scans: the first two day after injury, the second one seven days after injury, and the third one 12 days after injury. A total of 13 healthy adults [6 females, age: 39.77 ± 15.13 years (mean ± standard deviation)] were also included in the study so as to statistically compare the quantitative metrics obtained from ICH patients to those of a normative sample.

MRI volumes were acquired at 3.0 T using a Trio TIM scanner (1 mm^3 voxel size, Siemens Corp., Erlangen, Germany). The acquisition protocol consisted of magnetization prepared rapid acquisition gradient echo (MP-RAGE) T_1-weighted imaging, fluid attenuated inversion recovery (FLAIR), turbo spin echo (TSE) T_2-weighted imaging, gradient recalled echo (GRE) T_2-weighted imaging, and DTI. For the latter, volumes with 21 diffusion gradient directions were acquired for Patients 1 and 2, and with 64 directions for Patient 3. A similar acquisition protocol was used for the healthy control subjects as well. For ICH patients, conventional CT scans were also acquired.

Image processing

Prior to any analysis, all MRI and DTI volumes were co-registered. Image processing was performed using the LONI Pipeline environment (pipeline.loni.usc.edu), including bias field correction, skull stripping, and volume co-registration. Hemorrhagic tissues were segmented from GRE volumes and edematous tissues were segmented from T_2 and FLAIR volumes. The procedure for pathology identification is described in detail elsewhere by Irimia et al. [16]. Briefly, non-hemorrhagic edema was identified from T_2-weighted GRE imaging and FLAIR, whereas large hemorrhagic lesions and micro-hemorrhages were identified from susceptibility-weighted imaging (SWI). Diffuse axonal injury (DAI) was found to be apparent in DTI volumes. This protocol for identifying TBI-related pathology as well as details on its validation is described more extensively in our previous publication [16]. 3D Slicer software was used to generate 3D models and visualizations of pathology. To co-register WM surface models to pathology models, FreeSurfer was utilized to segment healthy-appearing WM, grey matter (GM), and cerebrospinal fluid (CSF) from T_1–weighted volumes using methodologies described elsewhere [17]. TrackVis and Diffusion Toolkit were used to reconstruct fiber tracts from DTI volume via deterministic tractography.

Specifically, a brain mask was first created using FSL [18] to eliminate extra-cerebral noise. TrackVis was then used to reconstruct and render fiber tracts, which were subsequently loaded and viewed in 3D Slicer. In each subject, fiber tracts which did not intersect pathology-affected regions were discarded.

To reconstruct the CST, seed regions were placed in the brain stem and internal capsule, and the WM tracts intersecting these regions were isolated.

The mean fractional anisotropy (FA) of each ICH patient was compared to the distribution of mean FA values in the sample of healthy control subjects as follows. Firstly, for both ICH patients and healthy subjects, the mean FA over the brain stem portion of the CST was computed. The brain stem portion of the CST was defined as the portion of this tract which is located between (A) the inferior extremity of either thalamus (whichever is positioned lower along the inferior-superior axis) and (B) the superior extremity of either the left or right cerebellum (whichever is positioned higher along the same axis). In each subject, this portion of the CST was registered to the FA map, and the mean and standard deviation of the FA within the brain stem was computed.

Quantitative and statistical analyses

Lesion volumes were measured in cubic centimeters based on the pathology models rendered in 3D Slicer. The percentage of volumetric ICH resolution was calculated as $(v_{i+1} - v_i)/v_i$, where v_i and v_{i+1} are the volumes of the ICH lesion at times i and $i + 1$, respectively. To quantify the extent to which fibers were affected by pathology, the sum over the lengths of fibers which intersected the pathology was divided by the sum of the lengths of fibers in the whole brain, thus yielding the percentage of fibers in the brain which intersected the primary injury.

To infer whether and to what extent the mean FA in the brain stem portion of the CST were significantly different in each ICH patient compared to the normative sample of healthy adults, the Z score of each patient's mean FA with respect to the reference sample was computed at each time point. The statistical significance of the difference in mean FA values between every patient at each time point and the control sample was then quantified under the null hypothesis that no difference in this measure existed between the control sample and each ICH patient. p values were calculated based on the assumption that the computed Z score followed a standard-normal distribution with zero mean and unit variance. Both Z -scores and p values are reported.

Results

Initial and follow-up MRI scans are displayed in Figures 1 and 2, with the time of the scan indicated at the top of the figure. Figure 3 displays representative slices acquired from conventional CT to additionally illustrate the extent of the lesions present in each subject. In Figures 4 and 5, respectively, the results of the pathology segmentation at the initial and subsequent time points are displayed. WM models were created for each subject and displayed to provide an anatomical reference. Edema is shown in cyan, and blood is shown in red. Columns A and B display the WM fibers which intersect pathology-affected regions.

For each subject, an enlarged, representative view is displayed in column C for closer inspection.

For Patient 1, hyper-intensities in the initial FLAIR scan indicate the presence of edema in the tissue surrounding the hemorrhage and around the anterior horn of the right lateral ventricle. The GRE and T_2 sequences reveal the hemorrhagic lesion load better than the T_1-weighted scan. The right ventricle appears comparably smaller than the left one, suggesting that the hematoma is displacing surrounding tissue and that it is thereby exerting pressure upon the ventricle. This effect is more obvious in the trigone of the lateral ventricle. Assessment of the CSTs reveal that the fibers in the right CST at the level of the internal capsule are somewhat displaced by the edema towards the midline, a finding which is consistent with our previous descriptions. The two-week follow-up scans indicate significant resolution of the hemorrhage, with persisting —though reduced— edema. The left and right ventricles appear more similar in size with respect to the acute scan, and the right CST exhibits notable recovery in terms of its displacement.

The initial scans for patient 2 indicate severe hemorrhage in the left hemisphere. The level at which the axial slices are displayed also indicate the presence of a significant midline shift at the level of the thalamus. As observed in the previous case, the MR volumes indicate a reduction in ventricle volume. Whereas the right CST (figure 6) appears healthy, the left CST is directly impacted by the hematoma and could not, for this reason, be reconstructed up to the primary somatosensory cortex due to increased diffusion isotropy within the hemorrhagic region. By contrast, DTI tractography based on scans acquired at follow-up demonstrates successful reconstruction of the left CST. Information provided by the GRE sequence indicates a reduction in hematoma size.

Patient 3 suffered a hemorrhage in the insula of the left hemisphere. No significant midline shift is observed, in contrast to the previous subjects. The subsequent scans indicate reduction in hematoma volume, with edema persisting around the lesion. Reconstruction of the CST suggests the presence of mostly healthy-appearing fibers.

Table 1 displays the results of volumetric and WM fiber-related quantifications for each patient. The time of the scan is indicated at the top of each column. Patient 1 was found to have a total lesion load of 62.4 cm^3 at the acute time point. On follow-up, this volume was reduced to 34.2 cm^3, with a decrease in both hemorrhage and edema. The percentage of hemorrhage resolved was calculated to be 67.68%. The percentage of fibers affected was initially 22.53%, decreasing to 18.05% on follow-up. Patient 2 had an initial total lesion load of 88.51 cm^3, which decreased to 73.66 cm^3, with 64.7% of hemorrhage resolving between the first and second time points. The percentage of fibers affected was 27.32% initially, but increased to 36.53%. Finally, for Patient 3, lesion load was tracked across four time points. The initial volumes of hemorrhagic and edematous tissue were 39.83 cm^3 and 10.59 cm^3, respectively. Whereas the size of the hemorrhage decreased to 16.03 cm^3 by the time of the final scan, edematous tissue increased in volume to 86.04 cm^3, resulting in a total lesion load of 102.07 cm^3 by the 12^{th} day after injury. The percentage of fibers affected by pathology decreased from 6.4% to 5.57% from the first to the third time point. Because DTI volumes were not collected on either Day 2 or Day 12 for clinically-related reasons, data for

these time points are unavailable. Inspection of Table 1 also indicates that the mean FA in the midbrain portion of the CST differed significantly between every ICH patient at each time point and that of the control sample. Because every Z score was observed to be negative, Table 1 also implies that the mean FA in the midbrain portion of the CST was significantly lower in each ICH patient and at every time point after injury compared to the reference sample of healthy control subjects.

Discussion

This study demonstrates an approach in which perilesional fibers can be selectively extracted and visualized based on MRI and DTI scans in ICH patients. Given that mechanical pressure due to mass effects can alter the anatomical paths of WM fibers, the ability to track pathology-affected fibers over the evolution of injury is relevant to the study of ICH. The modeling of hemorrhagic and edematous pathology provides useful knowledge on injury location with respect to brain tissue landmarks. This is relevant when considering that extravased blood components released after ICH impose cytotoxic, pro-oxidative, and pro-inflammatory effects on nearby viable brain cells [19]. In the case of edema, coagulation enzymes such as thrombin, which is produced in response to hemorrhage, have been shown in both animal and human studies to induce a variety of negative effects, among which are edema formation [1,20]. Thus, the generation of 3D pathology models is informative when targeting affected regions for preventive treatment.

In all three cases analyzed in this study, the amount of hemorrhage was observed to decrease between the initial and final scans. Conversely, cerebral edema was observed to progressively increase for Patients 2 and 3, which may be a cause for the increase in percentage of affected fibers in the case of Patient 2. This finding, however, is consistent with secondary brain injury mechanisms, which may impose pathophysiological effects leading to increases in cytotoxic or vasogenic edema [21,22].

As previously discussed, the CST is frequently studied in ICH cases due to the critical function of the former in voluntary fine motor control [2,14]. For that reason, our framework includes the ability to model the CST explicitly, which provides further detail on how injury has affected the ICH patient. For example, several authors have extrapolated that rapid and good recovery after stroke is associated with the resolution of factors such as peri-lesional edema or inflammation, whereas slow but good recovery is associated with brain plasticity [23-25]. Extending upon this finding, Kwon et al. [26] suggested that the former scenario can be attributed to the preservation of the CST over the course of injury, whereas the latter case can be attributed to recovery of the CST. The finding that every ICH patient had lower mean FA in the midbrain portion of the CST at each time point after injury may suggest appreciable atrophy in the midbrain section of this functionally-prominent bundle of WM fibers, which is consistent with previous findings of WM degeneration in ICH patients [27].

The utility of the methodology presented in this study is not restricted to the ability to perform visual observations. By placing fiducial markers in key regions of interest, it is also possible to use the approach proposed here to quantify fiber displacement across various time points. The challenge, however, would be to first devise a method whereby the same

fiber tracts located in some given anatomical region can be reliably identified across time points. Since tractography is initiated from seed regions, the reconstructed fibers may vary depending upon scan quality or upon physiological factors such as water anisotropy.

A final consideration is the limitation of DTI metrics such as fractional anisotrophy (FA) to describe WM property dynamics in peri-lesional regions. Particularly, given some location affected by edema immediately after injury, one might expect FA in such a region to decrease at first [28], and then gradually to increase as hematoma volume decreases. This is because the typical lesion pattern in ICH consists of a hemorrhagic core surrounded by non-hemorrhagic edema. However, in our case studies, average FA measured in peri-lesional regions indicated insignificant changes between the acute phase and at follow-up. On one hand, this may suggest lack of recovery. On the other hand, our case studies suggest that, when the amount of cerebral edema increases subsequent to the acute stage of ICH, the longitudinal comparison of FA values measured at locations within peri-lesional tissue may not be indicative of recovery due to the poor predictability of lesion shape dynamics. Nevertheless, the use of DTI metrics is a potentially useful direction for future applications to the study of ICH.

Conclusion

By utilizing DTI in conjunction with conventional structural imaging sequences, it is possible to selectively visualize fibers affected by injury pathology and to quantify the effect of the latter upon the former. Traditional methods of placing seed regions of interest (ROI) in pathology-affected regions can limit the tractography-based reconstruction to fibers which only pass through the selected voxels in the ROI. Thus, one drawback of DTI tractography is that some given reconstructed fiber bundle may cover only a portion of the tract of interest, as in the case of ROIs anatomically located within the CST. On the other hand, the approach described here allows one to reconstruct entire fasciculi such as the CST, and then to calculate fibers which intersect pathology-affected regions. This strategy is applicable to any WM structure. Furthermore, the results obtained from 3D ICH analysis can be helpful for assessing longitudinal changes in the locations of WM structures from the acute to the chronic stage.

Acknowledgments

We wish to thank the dedicated staff of the Institute for Neuroimaging and Informatics at the University of Southern California.

This work was supported by the National Institutes of Health, grants 2U54EB005149-06 “National Alliance for Medical Image Computing: Traumatic Brain Injury – Driving Biological Project” to J. D. V. H., and R41NS081792-01 “Multimodality Image Based Assessment System for Traumatic Brain Injury”, sub-award to J. D. V. H, and by the National Institute of Neurological Disorders and Stroke, grant P01NS058489 to P.M.V.

References

1. Xi G, Keep RF, Hoff JT. Mechanisms of brain injury after intracerebral haemorrhage. Lancet Neurol. 2006; 5(1):53–63. [PubMed: 16361023]

2. Koyama T, Tsuji M, Miyake H, Ohmura T, Domen K. Motor outcome for patients with acute intracerebral hemorrhage predicted using diffusion tensor imaging: an application of ordinal logistic modeling. J Stroke Cerebrovasc Dis. 2012; 21(8):704–11. [PubMed: 21511497]

3. Daverat P, Castel JP, Dartigues JF, Orgogozo JM. Death and functional outcome after spontaneous intracerebral hemorrhage. A prospective study of 166 cases using multivariate analysis. Stroke. 1991; 22(1):1–6. [PubMed: 1987664]

4. Morgenstern LB, Hemphill JC 3rd, Anderson C, Becker K, Broderick JP, Connolly ES Jr, Greenberg SM, Huang JN, MacDonald RL, Messe SR, et al. Guidelines for the management of spontaneous intracerebral hemorrhage: a guideline for healthcare professionals from the American Heart Association/American Stroke Association. Stroke. 2010; 41(9):2108–29. [PubMed: 20651276]

5. Broderick JP, Brott TG, Duldner JE, Tomsick T, Huster G. Volume of intracerebral hemorrhage. A powerful and easy-to-use predictor of 30-day mortality. Stroke. 1993; 24(7):987–93. [PubMed: 8322400]

6. Schonberg T, Pianka P, Hendler T, Pasternak O, Assaf Y. Characterization of displaced white matter by brain tumors using combined DTI and fMRI. Neuroimage. 2006; 30(4):1100–11. [PubMed: 16427322]

7. Lin DD, Filippi CG, Steever AB, Zimmerman RD. Detection of intracranial hemorrhage: comparison between gradient-echo images and b(0) images obtained from diffusion-weighted echo-planar sequences. AJNR Am J Neuroradiol. 2001; 22(7):1275–81. [PubMed: 11498414]

8. Kidwell CS, Chalela JA, Saver JL, Starkman S, Hill MD, Demchuk AM, Butman JA, Patronas N, Alger JR, Latour LL, et al. Comparison of MRI and CT for detection of acute intracerebral hemorrhage. JAMA. 2004; 292(15):1823–30. [PubMed: 15494579]

9. Witwer BP, Moftakhar R, Hasan KM, Deshmukh P, Haughton V, Field A, Arfanakis K, Noyes J, Moritz CH, Meyerand ME, et al. Diffusion-tensor imaging of white matter tracts in patients with cerebral neoplasm. J Neurosurg. 2002; 97(3):568–75. [PubMed: 12296640]

10. MacDonald CL, Dikranian K, Bayly P, Holtzman D, Brody D. Diffusion tensor imaging reliably detects experimental traumatic axonal injury and indicates approximate time of injury. The Journal of neuroscience. 2007; 27(44):11869–76. [PubMed: 17978027]

11. Mori S, van Zijl PC. Fiber tracking: principles and strategies - a technical review. NMR in biomedicine. 2002; 15(7-8):468–80. [PubMed: 12489096]

12. Skudlarski P, Jagannathan K, Calhoun VD, Hampson M, Skudlarska BA, Pearlson G. Measuring brain connectivity: diffusion tensor imaging validates resting state temporal correlations. NeuroImage. 2008; 43(3):554–61. [PubMed: 18771736]

13. Dauguet J, Peled S, Berezovskii V, Delzescaux T, Warfield SK, Born R, Westin CF. Comparison of fiber tracts derived from in-vivo DTI tractography with 3D histological neural tract tracer reconstruction on a macaque brain. NeuroImage. 2007; 37(2):530–8. [PubMed: 17604650]

14. Jung YJ, Jang SH. The fate of injured corticospinal tracts in patients with intracerebral hemorrhage: diffusion tensor imaging study. American Journal of Neuroradiology. 2011; 33(9): 1775–1778. [PubMed: 22492571]

15. Kusano Y, Seguchi T, Horiuchi T, Kakizawa Y, Kobayashi T, Tanaka Y, Seguchi K, Hongo K. Prediction of functional outcome in acute cerebral hemorrhage using diffusion tensor imaging at 3T: a prospective study. AJNR Am J Neuroradiol. 2009; 30(8):1561–5. [PubMed: 19556354]

16. Irimia A, Chambers MC, Alger JR, Filippou M, Prastawa MW, Wang B, Hovda DA, Gerig G, Toga AW, Kikinis R, et al. Comparison of Acute and Chronic Traumatic Brain Injury Using Semi-Automatic Multimodal Segmentation of MR Volumes. Journal of Neurotrauma. 2011; 28(11): 2287–2306. [PubMed: 21787171]

17. Dale AM, Fischl B, Sereno MI. Cortical surface-based analysis. I. Segmentation and surface reconstruction. Neuroimage. 1999; 9(2):179–94. [PubMed: 9931268]

18. Jenkinson M, Beckmann CF, Behrens TE, Woolrich MW, Smith SM. Fsl. Neuroimage. 2012; 62(2):782–90. [PubMed: 21979382]

19. Aronowski J, Zhao X. Molecular pathophysiology of cerebral hemorrhage: secondary brain injury. Stroke. 2011; 42(6):1781–6. [PubMed: 21527759]

20. Gebel JM, Brott TG, Sila CA, Tomsick TA, Jauch E, Salisbury S, Khoury J, Miller R, Pancioli A, Duldner JE, et al. Decreased perihematomal edema in thrombolysis-related intracerebral hemorrhage compared with spontaneous intracerebral hemorrhage. Stroke. 2000; 31(3):596–600. [PubMed: 10700491]
21. Donkin JJ, Vink R. Mechanisms of cerebral edema in traumatic brain injury: therapeutic developments. Curr Opin Neurol. 2010; 23(3):293–9. [PubMed: 20168229]
22. Barzo P, Marmarou A, Fatouros P, Hayasaki K, Corwin F. Contribution of vasogenic and cellular edema to traumatic brain swelling measured by diffusion-weighted imaging. J Neurosurg. 1997; 87(6):900–7. [PubMed: 9384402]
23. Demeurisse G, Demol O, Robaye E. Motor evaluation in vascular hemiplegia. Eur Neurol. 1980; 19(6):382–9. [PubMed: 7439211]
24. Saleh A, Schroeter M, Jonkmanns C, Hartung HP, Modder U, Jander S. In vivo MRI of brain inflammation in human ischaemic stroke. Brain. 2004; 127(Pt 7):1670–7. [PubMed: 15128622]
25. Jang SH. Unusual long-term motor recovery in a patient with corona radiata infarct. Neural Regeneration Resesearch. 2010; 5:1353–1356.
26. Kwon HG, Choi BY, Chang CH, Kim SH, Jung YJ, Jang SH. Recovery of an injured corticospinal tract during a critical period in a patient with intracerebral hemorrhage. NeuroRehabilitation. 2013; 32(1):27–32. [PubMed: 23422456]
27. Smith EE, Gurol ME, Eng JA, Engel CR, Nguyen TN, Rosand J, Greenberg SM. White matter lesions, cognition, and recurrent hemorrhage in lobar intracerebral hemorrhage. Neurology. 2004; 63(9):1606–12. [PubMed: 15534243]
28. Dervan L, Poliakov A, Friedman SD, Shaw D, Pihoker C, Roberts JS, Richards T, Marro K, Vavilala MS. Change in fractional anisotropy during treatment of diabetic ketoacidosis in children. Pediatr Res. 2014; 75(1-1):62–6. [PubMed: 24105411]

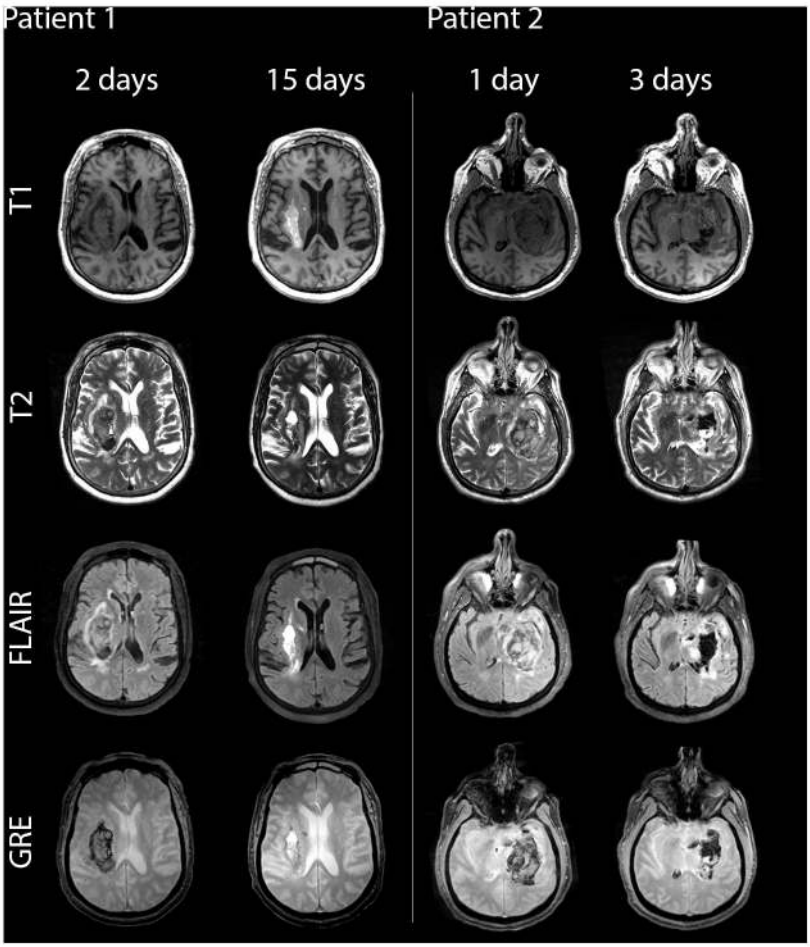

Figure 1.
MRI slices acquired at two different time points are displayed for Patients 1 and 2. Each row displays a different modality, i.e. T_1, T_2, FLAIR, and GRE.

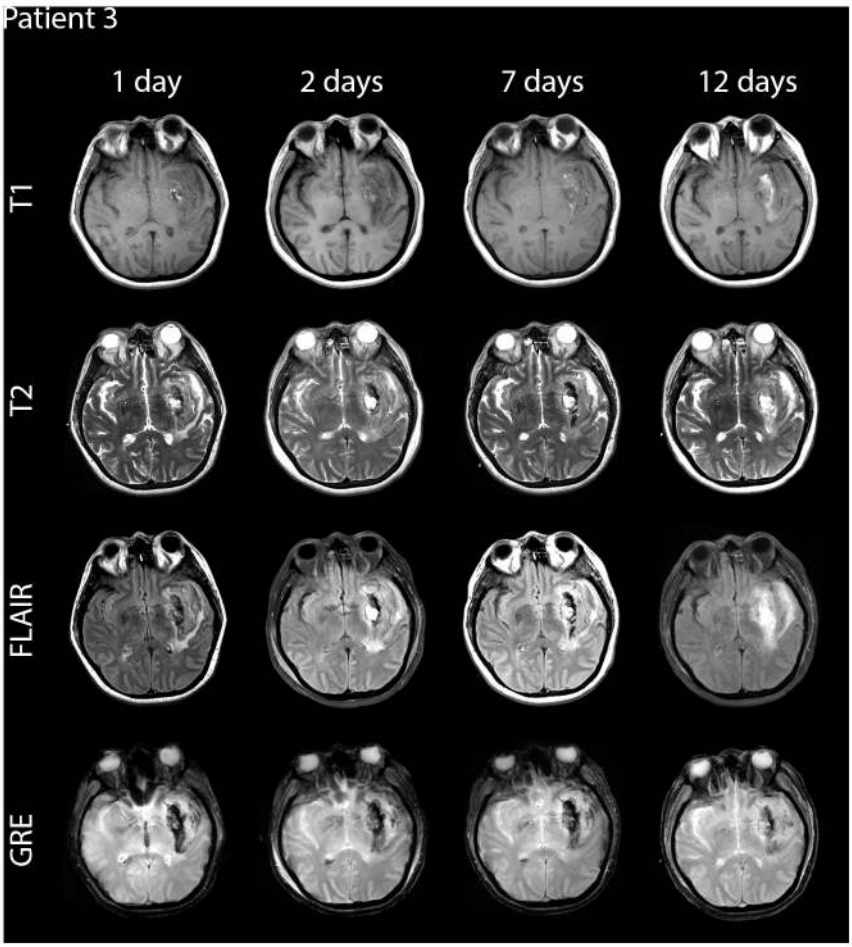

Figure 2.
MRI slices acquired from Patient 3. This patient received four separate scans, in contrast to only two scans in the previous two subjects.

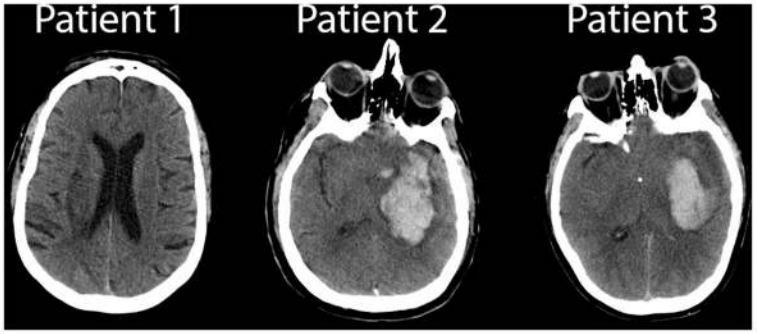

Figure 3.
Initial CT slices displaying the extent of hemorrhage. However, note that the integrity of major tracts such as the CST are not easily seen.

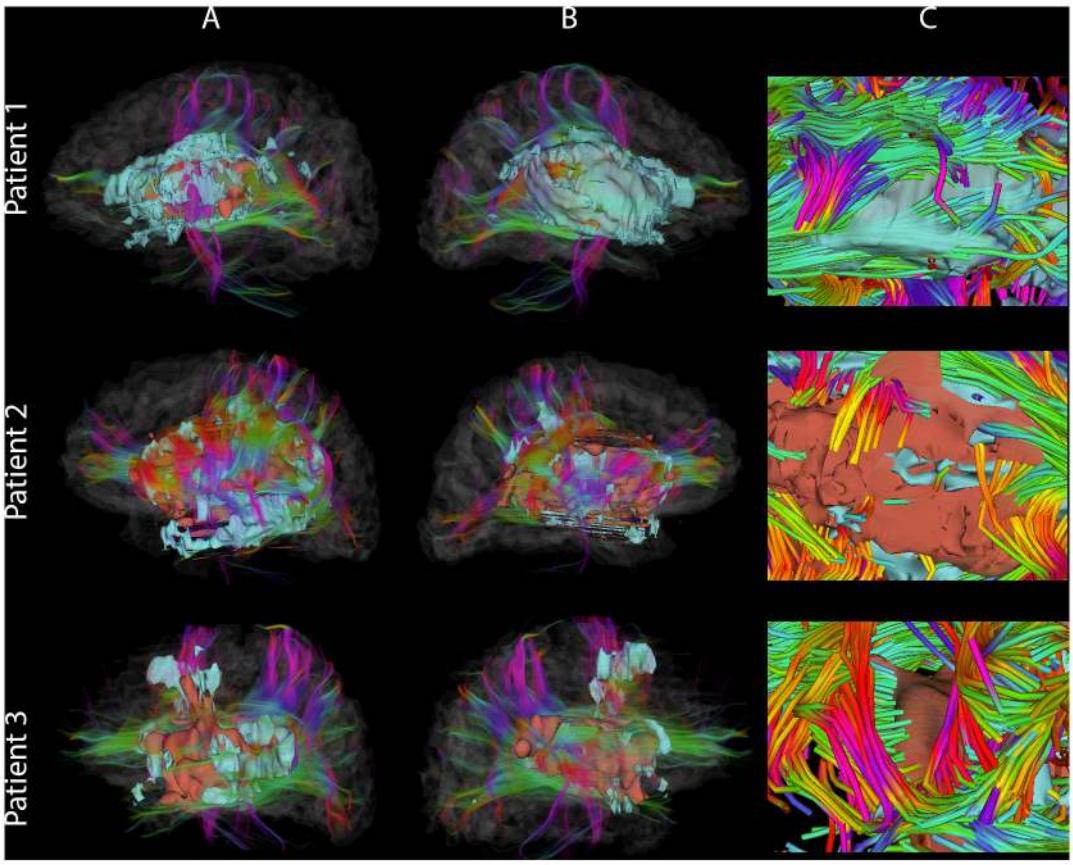

Figure 4.

The intersection between WM fiber tracts and the ICH pathology at the first time point is displayed in addition to 3D models of the pathology. Columns A and B display the left and right hemispheres, respectively. Column C displays an enlarged, representative view of the intersection between fibers and pathology-affected regions.

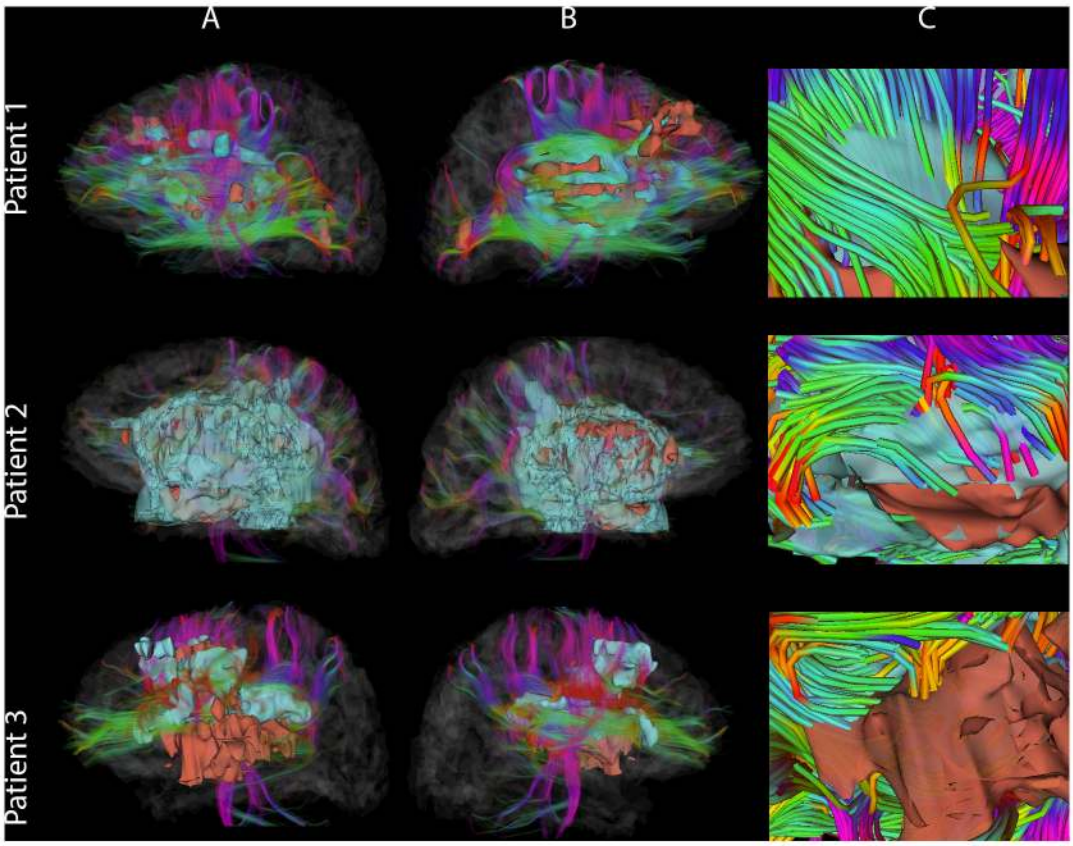

Figure 5.
Visualizations of fiber tracts intersecting the ICH pathology at the second time point.

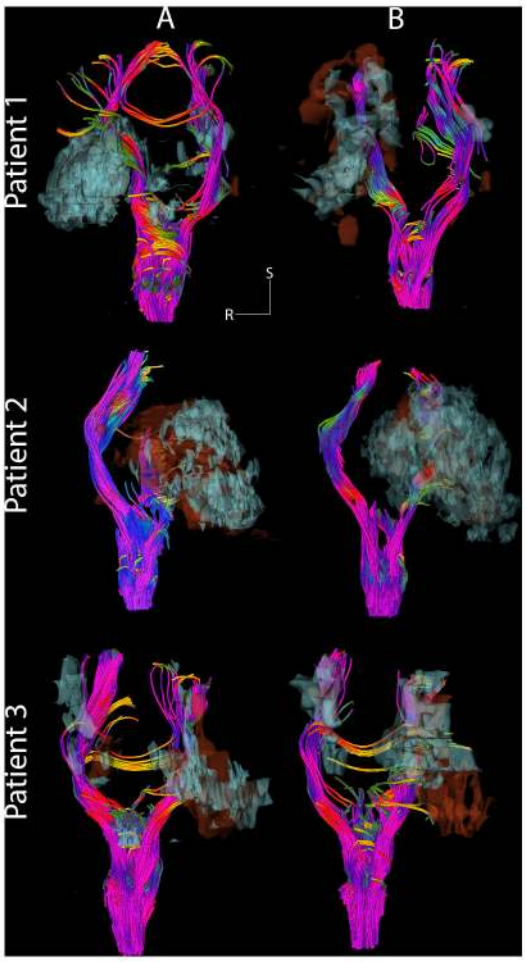

Figure 6.
The CST is explicitly modeled and displayed simultaneously with 3D models of ICH pathology. Columns A and B correspond to the acute and chronic scans, respectively.

Table 1

Quantification of ICH evolution. The post-injury time of each scan is indicated in days (d) at the top of each column. Volumes are quoted in cm^3, with the percent resolution of hemorrhage also being indicated at the bottom of the table. Blank entries indicate unavailability of the data (see text). The formula for the calculation of the percentage of fibers intersecting the ICH pathology is indicated in the Methods section.

Patient		**1**		**2**		**3**			
post-injury day		3	15	1	3	1	2	7	12
edema volume [cm3]		29.73	23.64	16.66	48.3	10.59	22.37	29.83	86.04
hemorrhage volume [cm3]		32.67	10.56	71.85	25.36	39.83	46.56	17.22	16.03
lesion load [cm3]		62.4	34.2	88.51	73.66	50.42	68.93	47.05	102.07
midline shift [mm]		4.08	4.72	5.47	4.51	0.74	1.75	0.44	1.14
FA of midbrain CST	μ	0.3796	0.3823	0.3921	0.372	0.4242	-	0.4547	-
	σ	0.1485	0.2013	0.1819	0.1596	0.1866	-	0.1815	-
	z	-7.038	-6.8612	-6.2422	-7.5118	-4.2146	-	-2.288	-
	p	< 0.00001	< 0.00001	< 0.00001	< 0.00001	< 0.00001	-	< 0.00001	-
hemorrhage amount resolved [%]		-	67.68	-	64.7	-	-	-	59.75
WM fibers affected [%]		22.53	18.05	27.32	36.53	6.43	-	5.57	-

Brain Inj. Author manuscript; available in PMC 2015 May 21.